Journal of Magnetic Resonance 209 (2011) 39–46

Contents lists available at ScienceDirect

Journal of Magnetic Resonance

journal homepage: www.elsevier.com/locate/jmr

T_2 distribution mapping profiles with phase-encode MRI

Oleg V. Petrov [a,*], Geir Ersland [b], Bruce J. Balcom [a]

[a] MRI Research Centre, Department of Physics, University of New Brunswick, Fredericton, Canada
[b] Department of Physics and Technology, University of Bergen, Norway

ARTICLE INFO

Article history:
Received 15 June 2010
Revised 15 December 2010
Available online 19 December 2010

Keywords:
T_2 mapping
SPRITE
Spin-echo SPI
Porous solids

ABSTRACT

Two 1-D phase-encode sequences for T_2 mapping, namely CPMG-prepared SPRITE and spin-echo SPI, are presented and compared in terms of image quality, accuracy of T_2 measurements and the measurement time. The sequences implement two different approaches to acquiring T_2-weighted images: in the CPMG-prepared SPRITE, the T_2-weighting of magnetization precedes the spatial encoding, while in the spin-echo SPI, the T_2-weighting follows the spatial encoding. The sequences are intended primarily for T_2 mapping of fluids in porous solids, where using frequency encode techniques may be problematic either due to local gradient distortions or too short T_2. Their possible applications include monitoring fluid-flow processes in rocks, cement paste hydration, curing of rubber, filtering paramagnetic impurities and other processes accomplished by changing site-specific T_2.

1. Introduction

Most methods for measuring spatially-resolved T_2 (T_2 mapping) employ multiple-echo pulse sequences with frequency encode (readout) gradients [1,2]. Being suitable for homogeneous soft systems, those methods may be inappropriate for T_2 mapping in porous solids, such as reservoir rocks, cement pastes and other building materials. Susceptibility contrast in these samples, as well as sample holders, can readily spoil the uniformity of read-out gradients and thus distort the image [3]. Another difficulty arises if T_2 is short (as is often the case for fluids in porous solids) and requires, to be measured, a short echo period. The latter is hard to achieve in frequency-encode sequences, where the echo period is limited by the readout gradient's duration.

Purely phase-encode (or constant-time imaging) techniques can eliminate, or at least diminish, these difficulties. The phase encoding is insensitive to the susceptibility contrast, as it relies on a regular increment of the gradient's strength rather than on the gradient's uniformity. Besides, it does not necessarily require for the gradient pulse to be rectangular to provide a uniform sampling of k-space. The latter allows one to reduce the gradient pulse duration and hence the echo acquisition time considerably.

The phase-encode approach is well suited to a scheme where the magnetization is partially relaxed prior to the spatial encoding, by applying a regular CPMG pulse train. The advantage of such a scheme over multi-echo imaging is that it provides, in principle, the same range of measurable T_2 as a regular CPMG experiment. Hence, we present pulse sequences for both schemes. In their current versions, the sequences are one-dimensional. This is entirely satisfactorily for their use studying fluid behavior in porous media, which is the application of greatest interest to us. Their extension to 2-D will be the subject of future research.

2. Concept of T_2 mapping

On the experimental side, measuring spatially-resolved T_2's consists of acquiring a series of T_2-weigthed images with site-dependent relaxation rates. Then one can resolve the individual decays into a number of exponential components (T_2 distributions) by means of the inverse Laplace transform (ILT) or compute several forms of average T_2 without the inversion of relaxation data [4–6] for further analysis. Given T_2 decays, one can also correct the image intensity for a T_2 contrast, either by means of back-extrapolation of the decays or, more reliably but more laboriously, by integration of T_2 distributions.

As mentioned in the introduction, there may be two different ways to obtain the series of T_2-weighted images. In one scheme, the T_2-weighting precedes the spatial encoding (Scheme A in Fig. 1). The T_2-weighting is achieved by applying a regular CPMG pulse train, and the spatial-encoding sequence is chosen such as to provide an image intensity proportional to the CPMG-prepared magnetization. To obtain the required number of T_2 points, the experiment is repeated with different numbers of pulses in the CPMG train, hence the experiment's time proportional to the T_2 dimension. In the other scheme, the T_2-weighting follows the spatial encoding (Scheme B in Fig. 1). In this case, all T_2 points are acquired in one scan, and the experiment's time only weakly depends on the T_2 dimension. This scheme, therefore, provides a shorter

* Corresponding author.
E-mail address: opetrov@unb.ca (O.V. Petrov).

1090-7807/$ - see front matter © 2011 Elsevier Inc. All rights reserved.
doi:10.1016/j.jmr.2010.12.006

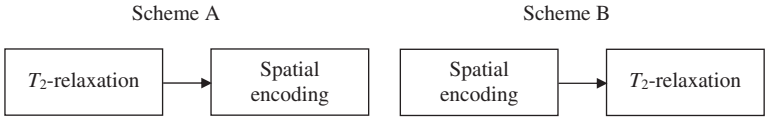

Fig. 1. Schematic of the T_2 distribution mapping measurements.

acquisition time than Scheme A whenever the image dimension is less than the number of T_2 points.

3. SPRITE with CPMG-prepared magnetization (Scheme A)

Fig. 2a presents a pulse sequence that implements Scheme A. The sequence employs for the spatially-encoding part SPRITE (Single Point Ramped Imaging with T_1 Enhancement) with double-half k-space (DHK) sampling [7]. The DHK SPRITE has been chosen for two reasons. First, it is one of the fastest purely phase-encode techniques, enabling full k-space acquisition in two scans. Second, it does not introduce an additional T_2-weight into the signal. The magnetization evolves under the CPMG sequence with a variable number of refocusing pulses and then is stored along the z-axis. Then the DHK SPRITE is applied to sample one half of a k-space signal, with the other half sampled with the next scan. To remove the steady-state component from a SPRITE signal (which is not proportional to the CPMG-prepared magnetization in general [7]), each of these scans is repeated twice: with a positive and negative z-storage, afterwards the difference signal is obtained [8].

The difference signal's intensity is given by

$$M_{xy}(n) = 2M_z(0)\sin\alpha[\cos\alpha, e^{-TR/T_1}]^{n-1} \quad (1)$$

where n is the number of the SPRITE pulse; $M_z(0) = M_0 e^{-m2\tau/T_2}$ the prepared z-magnetization after a m-pulse CPMG sequence with 2τ period; M_0 the equilibrium z-magnetization; α the SPRITE flip angle; and t_p the encoding time. The flip angle is set such as to provide a full-excitation of frequencies introduced by the gradient [9]

$$\alpha = \frac{90^\circ}{t_{90}} t_\alpha \leqslant \frac{90^\circ}{t_{90}} \frac{t_p}{N}, \quad (2)$$

where t_α and t_{90} are α- and 90°-pulse durations, respectively, and N is the total number of α-pulses in the DHK SPRITE sequence (that is, half the image dimension). For $t_p = 100$ μs, $N = 32$ and $t_{90} = 19$ μs used in this work, Eq. (2) gives $\alpha = 15^\circ$. One might prefer, however, using lower flip angles to reduce the blurring of the image due to the factor $(\cos\alpha)^{n-1}$ in (1).

The small excitation angle in SPRITE, hence a low SNR, is one of the shortcomings of the scheme. This is all the more problematic given that the majority of T_2 measurements in porous solids are carried out on low-field systems with a low sensitivity. Acquiring more than one point after α-pulses does help to increase SNR [10]; however, this approach requires a special (non-FFT) processing of acquired data, and we do not apply it here for sake of simplicity. Another disadvantage of the sequence is that the experiment time is proportional to the T_2 domain dimension. It may, therefore, take a rather long while to acquire the number of T_2 points required for ILT (typically, greater than 100). This number can be reduced considerably, however, if one measures the geometric mean T_2 without inversion of data, which requires fewer points than ILT [4]. The harmonic mean T_2 can be computed from the initial slope of a relaxation decay by using only as many initial data points as required for reliable differentiation and back-extrapolation. If it is only this measure of relaxivity that is of interest, then the acquisition will not take long.

The above-mentioned blurring of the image must be thought as a drawback of the method, too. On the other hand, it has the following considerable benefits. First, it provides, in principle, the same range of measurable T_2 as a regular CPMG sequence. This may be important when measuring T_2 in clay-bound water in reservoir rocks or gel water in cement-based materials, which may be well under 1 ms (see below). Second, it gives the first image already after four scans, so that one can control and optimize the image quality at very early stages of the experiment.

4. Spin-Echo SPI (Scheme B)

A Spin-Echo Single Point Imaging (SE-SPI) sequence, shown in Fig. 2b, implements Scheme B of T_2 mapping where the spatial encoding precedes the T_2 relaxation (see Fig. 1). In SE-SPI, the magnetization is phase encoded within the first pulse interval τ_0

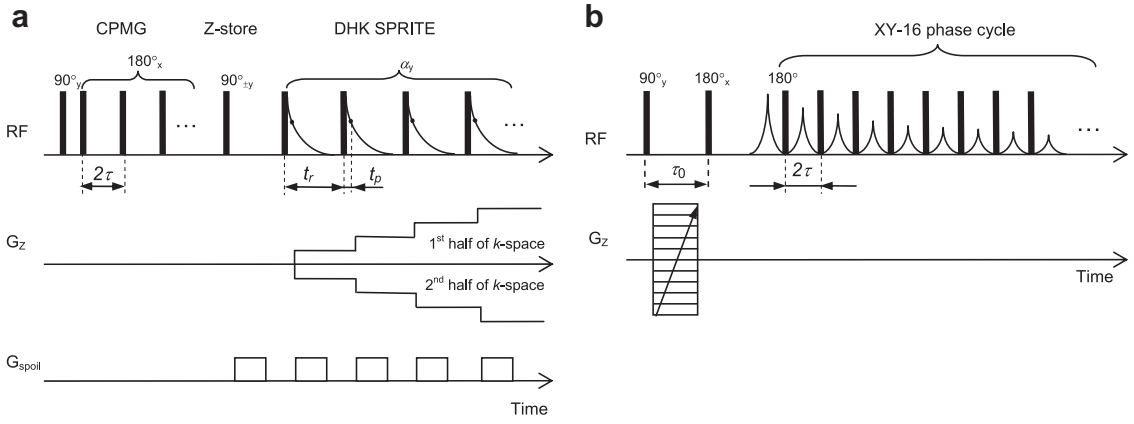

Fig. 2. (a) The CPMG-prepared double-half k-space SPRITE with alternating z-storage. Time intervals used were: $\tau = 0.2$ ms, $T_R = 1$ ms, $t_p = 0.1$ ms, and $\alpha = 10^\circ$. The spoiler-gradients dephase partially recovered longitudinal magnetization brought into the xy-plane by a z-storage pulse; otherwise it would interfere with the acquired signal. (b) The spin-echo SPI sequence. The magnetization is phase encoded during the first pulse interval with $\tau_0 = 0.8$ ms and then readout through multiple refocusing with $\tau = 0.2$ ms. To preserve the introduced phase shift upon refocusing, an XY-16 phase cycle is applied. A hard (full-excitation) 90-degree pulse is used, which is in contrast to the multi-echo sequences intended for whole-body imagers employing soft (slice-selective) 90° pulses [1].

and then readout through multiple refocusing with the period τ, $\tau < \tau_0$. To preserve both x- and y-components of magnetization while refocusing, an XY-16 phase cycle is applied [11]. Once the k-space sampling is complete, data points from each echo will give a profile with a particular T_2 weight. The signal intensity after the mth echo is given by

$$M_{xy}(m) = M_0 e^{-2\tau_0/\widetilde{T}_2} e^{-(m-1)2\tau/T_2} \quad (3)$$

where m is the echo number and $\widetilde{T}_2$ is the relaxation constant for the first echo interval $2\tau_0$ (usually $\widetilde{T}_2 \leqslant T_2$, see below).

To increase SNR, one acquires as many echo points as possible for given τ and dwell time. The profiles obtained from different echo points are then added up to yield a single profile. For an acquisition window much shorter than T_2^*, the intensity of such cumulative profile will be roughly proportional to the number of echo points used.

The multi-point acquisition, combined with the full-excitation pulses ($\alpha = 90°$), makes this sequence superior to the CPMG-prepared SPRITE for SNR. Furthermore, since the experiment time is now proportional to the number of k-space points (N) rather than T_2 points (M), this sequence is faster than the CPMG-prepared SPRITE whenever $N < M$. It also introduces no blurring to the image. A drawback is, however, that the presence of the phase-encode gradient between first two r.f. pulses, hence a relatively long τ_0, makes a difficulty for measuring short T_2 components of the signal. For diffusing spins, the long τ_0 also means a greater diffusion attenuation term in the relaxation constant (roughly $\propto\tau^2$), which may introduce the disproportion in the image intensity of slow- and fast-diffusing components.

A similar sequence (also named SE-SPI) has been demonstrated earlier by Li et al. [12]. Unlike the present one, however, the sequence by Li et al. has RARE-type bipolar phase encoding gradients in between refocusing 180-degree pulses, such that individual echo signals are encoded independently from one another. This gradient scheme was chosen because a regular CPMG phase cycle and pulse sequence had been employed, which is poor at preserving a phase coherence under multiple refocusing [13]. Therefore, Li et al. had to unwind the magnetization every time before applying a 180-degree pulse. Using the XY-16 phase cycle instead of CPMG allows us to encode the magnetization only once (after 90-degree pulse) and then to refocus it as many times as needed without loosing the phase shift introduced. Such a scheme seems preferable as it has the aforementioned gradient-stabilization restriction on the pulse spacing only for the very first echo, so one can acquire more echoes with higher peak intensities.

5. Test measurements

We first tested the sequences for their ability to measure a single-exponential T_2 relaxation. A 30 ml vial of water doped with $GdCl_3$ served as a test sample. Fig. 3a and b show axial profiles of the vial obtained by the two sequences. For comparison, profiles in the CPMG-prepared SPRITE experiments were acquired equidistantly and with the same interpulse delay $2\tau = 0.4$ ms as in the multi-echo sequence. To acquire a single profile in a CPMG-prepared SPRITE experiment took 30 s for the given number of scans (NS = 16), with 1024 profiles being acquired in 5 h. This contrasts with the SE-SPI experiment, which took only 5 min obtaining the same number of profiles and NS = 4. We note, though, that it was unnecessary to acquire all 1024 profiles in the CPMG-prepared SPRITE experiment, nor to use a constant echo increment, and it is the acquisition time per profile that is of principle interest. However, even with an optimized profile acquisition, the experimental time of the CPMG-prepared SPRITE would significantly exceed that of an SE-SPI sequence.

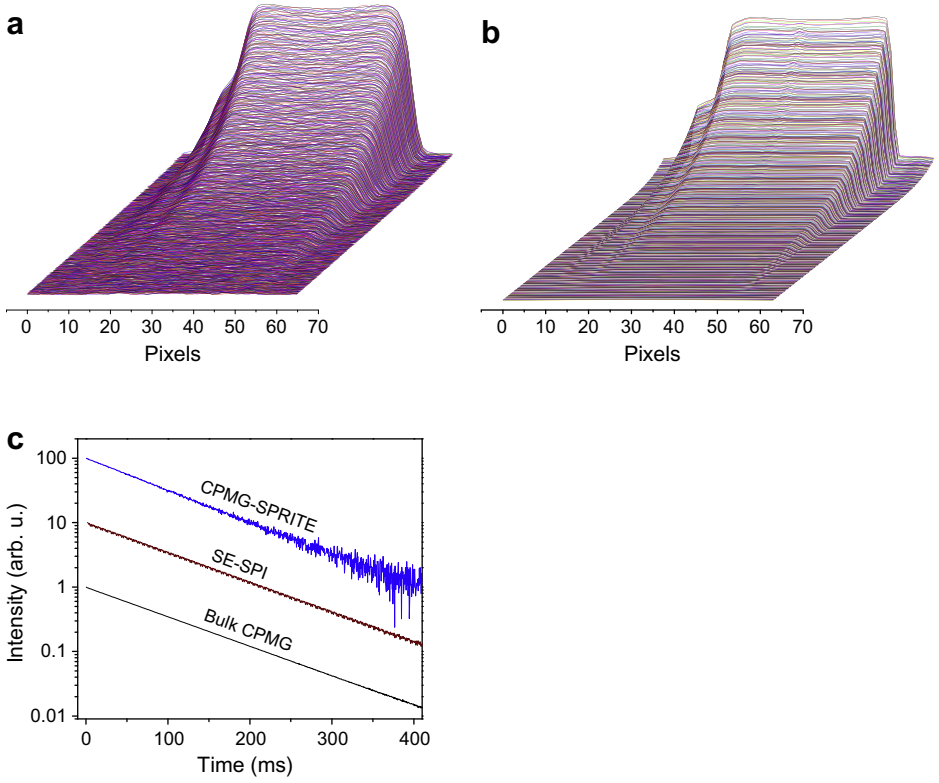

Fig. 3. Axial profiles of a 30 ml vial of $GdCl_3$-doped water, obtained by CPMG-prepared SPRITE (a) and SE-SPI (b) sequences. Panel (c) compares central pixel decays for these sequences; the decays have the same slope ($T_2 \sim 94$ ms), similar to a bulk CPMG measurement, but noticeably different SNR. (The decays are shifted on the y-axis for better comparison.)

Despite the fourfold increased number of scans, the profiles obtained by the CPMG-prepared SPRITE exhibit a lower SNR than their SE-SPI counterparts. As a result, pixel decays of the CPMG-prepared SPRITE profiles disappear in the noise already within less than two orders of magnitude decay (Fig. 3c). As discussed below, this could make it difficult to detect long T_2 components in T_2 distributions. Nevertheless, both sequences reproduce a single-exponential decay very well within the profile, with T_2 being consistent with the bulk CPMG measurement (Fig. 3c).

In the next set of tests, we examined the ability of the sequences to measure T_2 distributions in realistic rock samples. Test samples were two different sandstones, Berea sandstone (porosity φ = 21%) and Wallace sandstone (φ = 14%), cut into 5.2 × 2.5 cm cylinders and saturated with distilled water.

We consider the Berea sample first. Fig. 4a shows profiles of the Berea sample obtained with the CPMG-prepared SPRITE experiment. A single profile took approximately 2 min. (The increased acquisition time was due to longer T_1 (water was not doped) and lesser amount of water (φ = 21%) in the sample). To reduce the total experiment time, we skipped every other echo and acquired 483 profiles, in a 16 h acquisition. For comparison, Fig. 4b shows profiles obtained with the SE-SPI sequence; in that case 2048 profiles were acquired, and the experiment was 12 min for NS = 4. Fig. 4c shows T_2 distributions obtained from a central pixel's relaxation decays in the profiles shown in Fig. 4a and b, plotted along with a reference distribution from a bulk CPMG measurement. (Water in Berea exhibits a uniform T_2 relaxation over the sample; this makes the comparison of single-pixel and bulk T_2 distributions valid.) The bulk T_2 distribution in this sample appears to be unimodal, with a peak centered at 210 ms and the arithmetic mean T_2, $\langle T_2 \rangle$, equal to 120 ms. The SE-SPI experiment yields a distribution that coincides with the bulk for all T_2 values except the shortest ones, where it misses components below T_2 = 3 ms (yielding a longer $\langle T_2 \rangle$ = 140 ms). That is the consequence of the above-mentioned necessity to keep the first interpulse delay τ_0 long enough to contain the encoding gradients, which effectively eliminates short T_2 components. In its turn, the distribution from the CPMG-prepared SPRITE experiment misses T_2 components on the longer-T_2 side (see Fig. 4c), resulting in a shorter $\langle T_2 \rangle$ = 100 ms compared to the reference T_2 distribution. At present we have no definitive explanation for this effect but hypothesize it is due to poor SNR in this class of experiment and the inability of an ILT algorithm to recognize long T_2 components behind the noise.

The second test sample, a water-saturated Wallace sandstone, exhibits a bi-modal T_2 distribution, with the peaks centered at T_2 = 45 and 0.45 ms (Fig. 5c). The latter peak is most likely to belong to water absorbed in clay which Wallace sandstone contains in a considerable amount. This, combined with the low porosity (φ = 14%), makes the Wallace sample a good challenge to the techniques under study. Fig. 5a shows profiles of this sample obtained in the CPMG-prepared SPRITE experiment. Only 128 profiles were acquired, which took 9 h. A SE-SPI experiment took 12 min with 1200 profiles (Fig. 5b). T_2 distributions measured from those profiles demonstrate the same features as before. Namely, the distribution obtained from the SE-SPI experiment misses shorter T_2 components, while that from the CPMG-prepared SPRITE misses longer T_2 components.Our final test was a composite sample, comprising two pieces of Wallace sandstone: one piece saturated with water and the other piece saturated with heavy mineral oil. As for all test samples, the saturation was carried out by immersing a sandstone, preliminary dried at 120 °C in a vacuum oven, into a particular fluid and leaving it under vacuum for 12 h. Fig. 6a and b show profiles from both experiments, while Fig. 6c and d compare T_2 distributions in the water- and oil-saturated pieces, respectively. This test demonstrates, in particular, that SE-SPI introduces an essential disproportion to the signal intensity of water and oil. That is, being saturated in equal proportions by water and oil, the water-saturated half appears to contain less fluid than the oil-saturated piece. The disproportion is due to a greater diffusion attenuation of water signal during the first interpulse delay τ_0 (roughly $\propto D\tau_0^3$, where D is

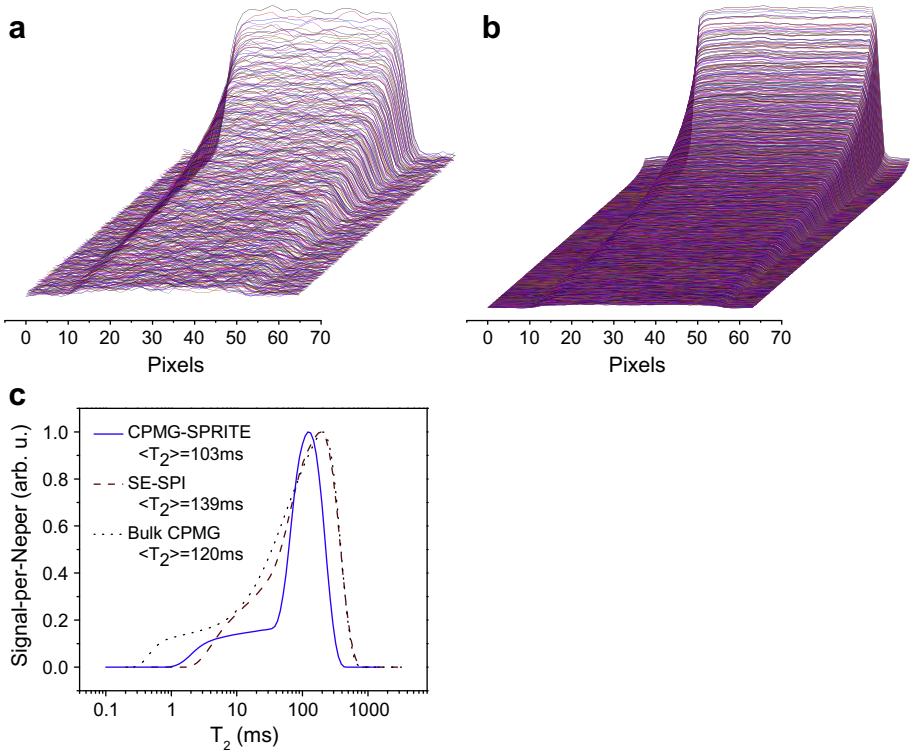

Fig. 4. Profiles of a cylindrical core plug of Berea sandstone saturated with water, from CPMG-prepared SPRITE (a) and SE-SPI (b) experiments. T_2 distributions measured from a central pixel's decays are plotted in (c) along with the bulk CPMG data. Due to a low sensitivity, the CPMG-prepared SPRITE looses the longest T_2 components behind the noise. In turn, SE-SPI cannot reveal short T_2's (<2 ms), due to the finite τ_0 (=0.8 ms). The distributions shown are normalized according to its peak intensity.

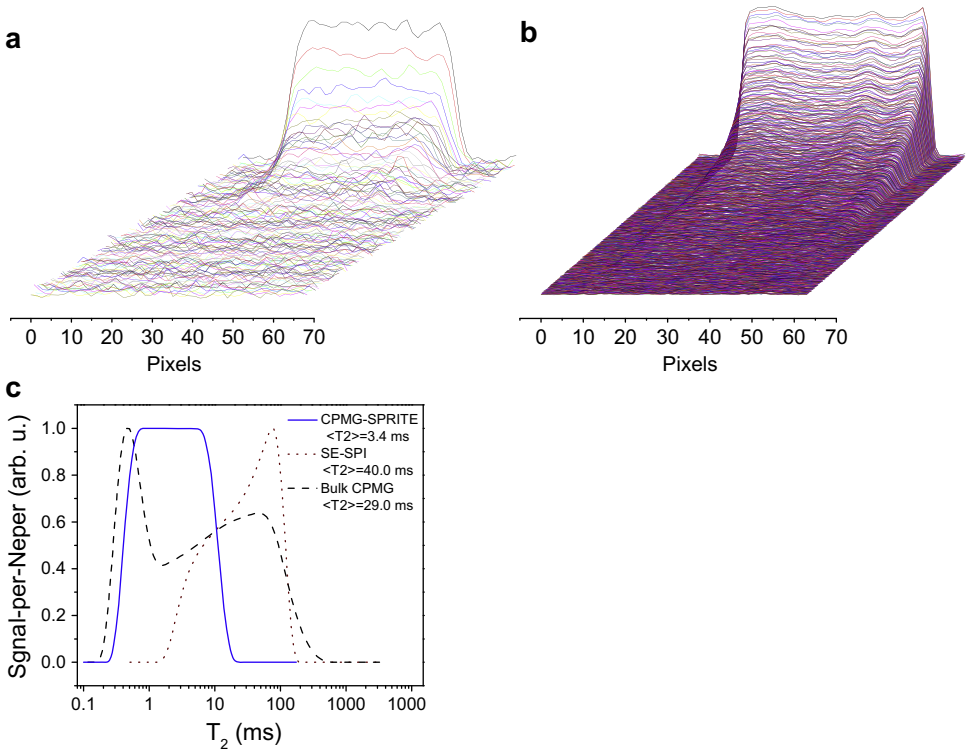

Fig. 5. Similar data set as in Fig. 4 but obtained for water-saturated Wallace sandstone. Again, the CPMG-prepared SPRITE misses the T_2 components longer than 20 ms, while SE-SPI cannot reproduce T_2 components shorter than 2 ms. The distributions shown are normalized according to their peak intensity.

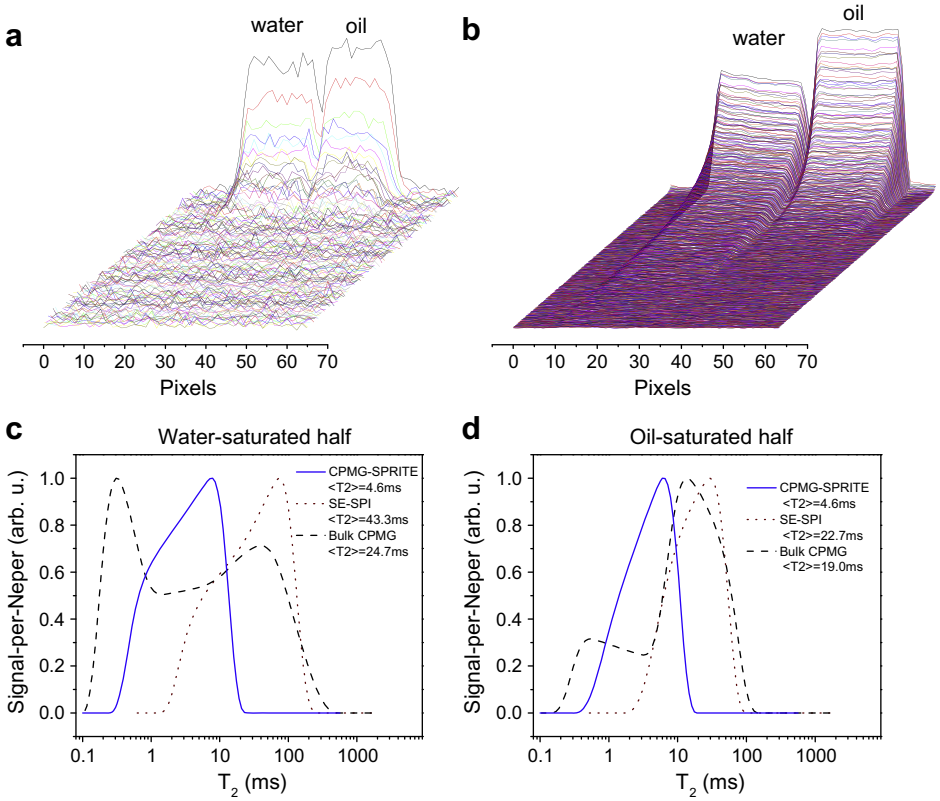

Fig. 6. Profiles of two pieces of Wallace sandstone, saturated with water and oil and put together, obtained from CPMG-prepared SPRITE (a) and SE-SPI experiment (b). On the panels (c) and (d) are compared the T_2 distributions in the water-saturated and oil-saturated halves, respectively. The distributions are normalized according to their peak intensity.

a diffusion coefficient). We notice that even the back-extrapolation of T_2 decays (or equivalently, the integration of T_2 distributions) will give the incorrect relative oil and water intensities in this case. In contrast, the CPMG-prepared SPRITE shows more realistic relative intensities for water- and oil-saturated pieces. Nevertheless, the SE-SPI measurements of T_2 distributions are in a very good agreement with the bulk T_2 measurements except for the shortest T_2 components. This suggests that given reference T_2 distributions, one can distinguish oil and water components along the sample, in cases where the T_2 distributions of individual components preserve their patterns under displacement processes.

6. Discussion

Despite the advantage of the unlimited echo spacing, the CPMG-prepared SPRITE seems impractical for 1-D T_2 mapping unless only a few T_2 points are required, or a signal is strong enough for both quick scans and a reliable long-T_2 component detection. Otherwise one will prefer the SE-SPI sequence as being much faster yet also providing better SNR. The only disadvantage of SE-SPI seems to be a finite first interpulse delay, τ_0, which contains the encoding gradient. Thus, the hardware used in this study requires at least 300–400 μs for the gradient to be established and another 300–400 μs delay after turning off the gradient to settle down eddy currents. Setting shorter delays results in distorted profiles. This limits a first echo detection time to 1.2–1.6 ms, which may be too long for detecting such short T_2 components as, e.g., clay-bound water in rocks or gel water in cement pastes. This limitation can be partially remedied by using faster rise time gradients and gradient waveform mapping for an appropriate pre-emphasis of gradient pulses.

The situation might be very different, however, if one wants to extend these sequences to higher image dimensionality. For the CPMG-prepared SPRITE, such an extension merely means replacing the 1-D DHK SPRITE with a 2-D spiral SPRITE [14] or a 3-D conical SPRITE [15], which will not entail a serious elongation of the experiment. In the case of SE-SPI, on the other hand, the naive extension to 2-D or 3-D would mean a N or N^2-fold increase in the number of scans, respectively. Although one can employ one of the scan-time reduction methods that allow reconstructing the image from incomplete datasets (see, e.g., [16–18]), it is not without complications.

Conventional pulse sequences for T_2 mapping in 2-D and 3-D employ the frequency encoding technique (see e.g. [1]), which gives a good SNR and short image acquisition time. These methodologies are to be preferred when one is exclusively concerned with long T_2 lifetimes distributions. Using modern hardware allows to keep the interecho spacing containing read-out gradients in those sequences as short as 5–10 ms [2], making it possible to detect T_2 down to 10 ms [19]. This may be, however, insufficient for analysis of reservoir rocks, cement-based materials or food systems where the information of interest is often contained within T_2 components shorter than 10 ms (see below).

Ultra-short echo time (UTE) imaging with a spiral readout has been recently employed for 2-D mapping of effective transverse relaxation T_2^* of knee cartilage with the shortest $T_2^* \sim 0.5$ ms [20], taking 5 min for one image. It is unclear, however, how to use UTE for T_2 distribution measurements other than in place of the MRI block in Scheme A in Fig. 1, which would be similar to the case of CPMG-prepared 2-D spiral SPRITE but with the latter replaced by a frequency-encoding MRI sequence. Native UTE T_2^* mapping is not applicable to porous media since it is the T_2 distribution that is important in these systems, not T_2^*. In porous media systems the T_2^* is greatly modified from T_2 due to microscopic inhomogeneous broadening caused by susceptibility mismatch of the rock matrix and pore fluid. Indeed, it is commonly observed that a single exponential T_2^* decay results from this susceptibility mismatch [21] in realistic reservoir rocks.

The present purely phase-encoding sequences, though much slower than phase/frequency-encoding ones, allows one to measure T_2 down to 0.3 ms (see Fig. 5c). The absence of read-out gradients between refocusing pulses in SE-SPI enables acquiring as many echo signals as in a regular CPMG sequence before they decay down to a noise level, which is necessary for reliable T_2 measurements [22]. Finally, as mentioned in the Introduction, there may be cases (when using samples with macroscopic magnetic susceptibility contrast, core holders, metallic pressure vessels) where applying read-out gradients is impracticable due to a gradient distortion, so that employing the purely phase-encoding technique becomes the only option.

The extension of the sequences to higher dimensions will be the subject of our future work. In their present 1-D versions, the sequences can be of interest for studying unidirectional processes in porous media, such as core flooding, drying, filtering and all other processes accomplished by changing site-specific T_2. Fluid-flow properties of porous media, such as permeability and irreducible water saturation, can be ascertained from these T_2 measurements, either from T_2 distributions or by utilizing different forms of average T_2 [5,23]. In the samples containing both oil and water phases, their content can be estimated from a multivariate analysis of T_2 relaxation curves [24]. It has also been reported that T_2 distributions of water in some particular sandstone and carbonate samples correlate with their pore size distributions [23], which offers a reasonable assurance that T_2 estimates a pore size.

To illustrate the applicability the SE-SPI technique, we describe in Appendix A a core flooding experiment where this technique is employed for measuring T_2 distributions in the oil phase (dodecane) along the core plug at different stages of water flooding. T_2 mapping of immiscible processes in porous media, in addition to the saturation map, reveals spatial information of phase occupancy in relation to pore sizes. The method may also be suitable for studies of miscible processes, for dispersion and diffusion studies, for enhanced oil recovery studies, and for characterizing porous rocks with regard to mass transfer between flowing fluids and stagnant fluids in dead-end pores.

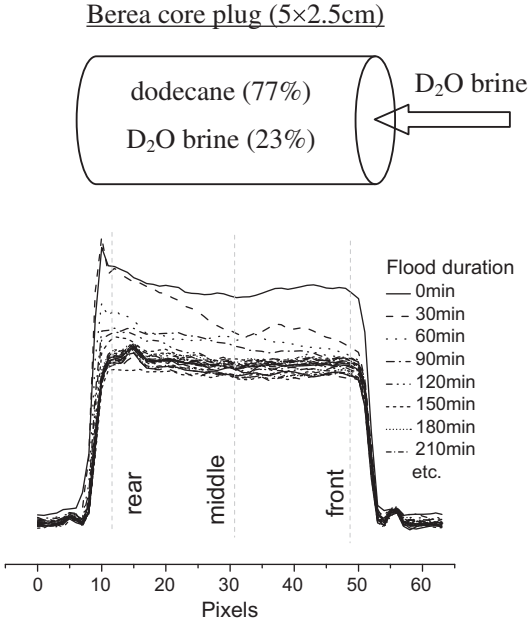

Fig. A1. The first-echo profiles from a SE-SPI dataset recorded during water (D_2O brine) flooding of water-wet Berea sandstone saturated with dodecane. The sample preparation is described in the text. The profiles reflect the residual dodecane distribution over the sample as the flooding proceeds. The dotted line show the sites at which T_2 distributions are reported in Fig. 8.

7. Conclusion

In this paper we have outlined two different T_2 mapping methodologies. The CPMG-prepared SPRITE method is biased against long T_2 signal components while the SE-SPI multi-echo method is biased against short T_2 signal components. The latter limitation is likely to be alleviated by better hardware performance. The utility of T_2 mapping measurements which yield viable and realistic T_2 distributions spatially resolved is shown through model sample experiments and a realistic core flooding example. We feel core flooding applications of T_2 distribution mapping will be particularly important since the T_2 distribution reports on fluid occupancy of the pore space.

8. Experimental

NMR measurements were carried out on an Oxford Instruments DRX spectrometer equipped with a 0.35 T horizontal bore magnet (ν = 15 MHz), at room temperature. The r.f. probe used was a 54-mm wide birdcage probe, a 90°-pulse duration being 19 μs. Composite pulses were employed for r.f. field inhomogeneity compensation [25]; namely, the sequences $45_{\pi/2}90_0 90_{3\pi/2}45_0$ for a composite 90° pulse, with the total duration of 57 μs, and $180_{2\pi/3}180_{4\pi/3}180_{2\pi/3}$ for a composite 180° pulse, with the total duration of 114 μs. The number of time-domain echo points acquired in SE-SPI experiments was 20. The rest of acquisition parameters are given in the figure captions. Prior to FFT, acquired k-space signals were multiplied by a Hanning window function to remove the Gibbs ringing at the profile edges.

T_2 distributions were measured by using a Laplace inverse transform algorithm UPEN [26].

Acknowledgments

This research was supported by NSERC of Canada, Petroleum Research Atlantic Canada, the Canada Chairs Program, and Conoco Phillips.

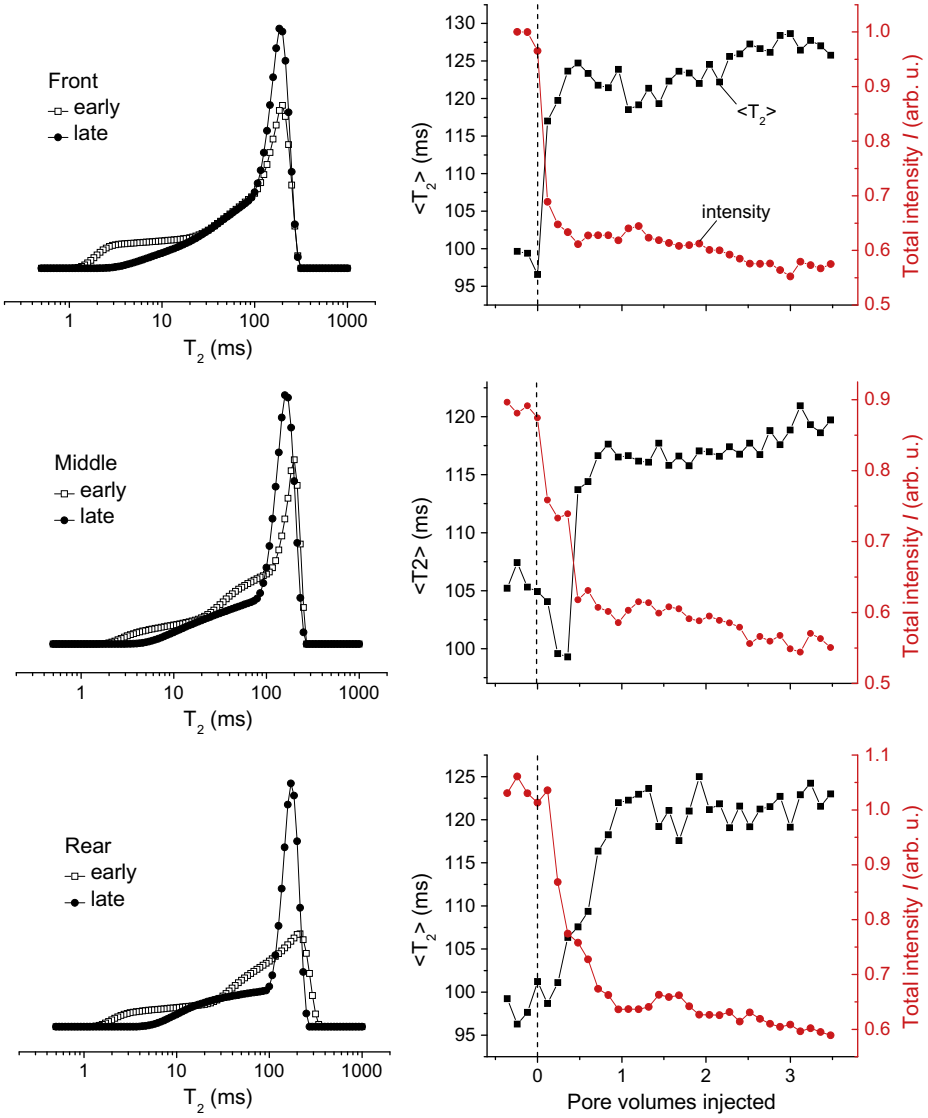

Fig. A2. On the left hand side (a) are shown T_2 distributions of dodecane in Berea measured near the front face, in the middle and near the rear face of the sample at early and late stages of flooding. The distributions are normalized to have an unit area. Note that the distributions loose short T_2's components as flooding proceeds. Arithmetic mean T_2, $\langle T_2 \rangle$, measured upon flooding are plotted on the right hand side (b) versus the residual dodecane's signal intensity, I (squares for $\langle T_2 \rangle$, circles for I); the plot demonstrates the inverse correlation between the quantities. The intensity is measured by the area under the T_2 distributions (which is equivalent to the back-extrapolation of T_2-decays).

Appendix A

The following example illustrates the use of the SE-SPI technique for monitoring water flooding of a core plug. A sample of Berea sandstone was first immersed into D_2O brine (2% wt. NaCl in D_2O) inside a vacuum chamber to be fully saturated with the brine and then dodecane was pumped through it until only 23% of D_2O brine is left. The sample models a natural water-wet oil reservoir rock with residual water saturation. During the experiment, the sample was flooded inside the magnet in a core holder with the same D_2O brine at a constant flow rate 1.2 ml/h, as shown in Fig. A1. The SE-SPI sequence was run every 30 min to monitor this process at three particular sites: near the front face, in the middle and near the rear face of the sample (see Fig. A1). We emphasize, however, that T_2 characteristic information is available from every pixel within the sample.

The water advancement is dominated by capillary forces; no sharp waterfront was observed. In a strongly water-wet system a dispersed front propagation is expected at low rates, with water spontaneously filling smaller pores first. As the flooding proceeds, the T_2 distribution of dodecane becomes narrower, mostly at the expense of short T_2 components (Fig. A2, the left hand side). The arithmetic mean T_2, $\langle T_2 \rangle$, obtained from these T_2 distributions, is plotted against the residual dodecane content on the right hand side of Fig. A2. One can see from the figure that $\langle T_2 \rangle$ and the residual dodecane content correlate inversely. To explain these results, we assume that short T_2 components of the distributions are due to pore surface effects on the dodecane relaxation. We then expect that the introduced water displaces dodecane mostly from smaller pores (where the capillary pressure is higher and thus the driving force of water imbibition is higher), so that the residual dodecane turns out to be trapped in larger pores where the surface relaxation effects are less pronounced. Such a behavior is indeed expected for a non-wetting phase [27]. Thickening the water layer adjacent to the pore wall during the waterflood would progressively isolate the dodecane phase from the surface, hence the observed increase of $\langle T_2 \rangle$.

References

[1] C.S. Poon, R.M. Henkelman, Practical T_2 quantitation for clinical-applications, J. Magn. Reson. Imaging 2 (1992) 541–553.
[2] T.J. Mosher, B.J. Dardzinski, Cartilage MRI T_2 relaxation time mapping: overview and applications, Semin. Musculoskeletal Radiol. 8 (2004) 355–368.
[3] O. Beuf, A. Briguet, M. Lissac, R. Davis, Magnetic resonance imaging for the determination of magnetic susceptibility of materials, J. Magn. Reson. Ser. B 112 (1996) 111–118.
[4] G.C. Borgia, V. Bortolotti, R.J.S. Brown, P. Fantazzini, A robust method for calculating geometric mean times from multiexponential relaxation data, using only a few data points and only a few elementary operations, Magn. Reson. Imaging 14 (1996) 895–897.
[5] G.C. Borgia, R.J.S. Brown, P. Fantazzini, Different "average" nuclear magnetic resonance relaxation times for correlation with fluid-flow permeability and irreducible water saturation in water-saturated sandstones, J. Appl. Phys. 82 (1997) 4197–4204.
[6] G.C. Borgia, V. Bortolotti, R.J.S. Brown, P. Fantazzini, A method for approximating fractional power average relaxation times without inversion of multiexponential relaxation data, Magn. Reson. Imaging 16 (1998) 625–627.
[7] I.V. Mastikhin, B.J. Balcom, P.J. Prado, C.B. Kennedy, SPRITE MRI with prepared magnetization and centric *k*-space sampling, J. Magn. Reson. 136 (1999) 159–168.
[8] A.A. Khrapitchev, B. Newling, B.J. Balcom, Centric-scan SPRITE magnetic resonance imaging with prepared magnetisation, J. Magn. Reson. 181 (2006) 271–279.
[9] S. Gravina, D.G. Cory, Sensitivity and resolution of constant-time imaging, J. Magn. Reson. Ser. B 104 (1994) 53–61.
[10] M. Halse, J. Rioux, S. Romanzetti, J. Kaffanke, B. MacMillan, I. Mastikhin, N.J. Shah, E. Aubanel, B.J. Balcom, Centric scan SPRITE magnetic resonance imaging: optimization of SNR, resolution, and relaxation time mapping, J. Magn. Reson. 169 (2004) 102–117.
[11] T. Gullion, The effect of amplitude imbalance on compensated Carr–Purcell sequences, J. Magn. Reson. Ser. A 101 (1993) 320–323.
[12] L. Li, H. Han, B.J. Balcom, Spin echo SPI methods for quantitative analysis of fluids in porous media, J. Magn. Reson. 198 (2009) 252–260.
[13] C.W. Windt, F.J. Vergeldt, H. Van As, Correlated displacement-T_2 MRI by means of a pulsed field gradient-multi spin echo method, J. Magn. Reson. 185 (2007) 230–239.
[14] P. Szomolanyi, D. Goodyear, B. Balcom, D. Matheson, SPIRAL-SPRITE: A Rapid Single Point MRI Technique for Application to Porous Media, Elsevier Science Inc., 2001. pp. 423–428.
[15] M. Halse, D.J. Goodyear, B. MacMillan, P. Szomolanyi, D. Matheson, B.J. Balcom, Centric scan SPRITE magnetic resonance imaging, J. Magn. Reson. 165 (2003) 219–229.
[16] J. Tsao, B. Behnia, A.G. Webb, Unifying linear prior-information-driven methods for accelerated image acquisition, Magn. Reson. Med. 46 (2001) 652–660.
[17] F. Wajer, Non-Cartesian MRI Scan Time Reduction through Sparse Sampling, Delft University of Technology, 2001.
[18] M. Lustig, D. Donoho, J.M. Pauly, Sparse MRI: the application of compressed sensing for rapid MR imaging, Magn. Reson. Med. 58 (2007) 1182–1195.
[19] M. Estilaei, A. MacKay, K. Whittall, J. Mayo, In vitro measurements of water content and T-2 relaxation times in lung using a clinical MRI scanner, J. Magn. Reson. Imaging 9 (1999) 699–703.
[20] Y. Qian, A.A. Williams, C.R. Chu, F.E. Boada, Multicomponent T2* mapping of knee cartilage: technical feasibility ex vivo, Magn. Reson. Med. 64 (2010) 1427–1432.
[21] Q. Chen, A.E. Marble, B.G. Colpitts, B.J. Balcom, The internal magnetic field distribution, and single exponential magnetic resonance free induction decay, in rocks, J. Magn. Reson. 175 (2005) 300–308.
[22] K.P. Whittall, A.L. MacKay, D.K.B. Li, Are mono-exponential fits to a few echoes sufficient to determine T-2 relaxation for in vivo human brain?, Magn Reson. Med. 41 (1999) 1255–1257.
[23] G.R. Coates, L. Xiao, M.G. Prammer, NMR Logging: Principles and Applications, Halliburton Energy Services, Houston, 1999.
[24] O.V. Petrov, J. Hay, I.V. Mastikhin, B.J. Balcom, Fat and moisture content determination with unilateral NMR, Food Res. Int. 41 (2008) 758–764.
[25] M.H. Levitt, Composite pulses, Prog. Nucl. Magn. Reson. Spectrosc. 18 (1986) 61–122.
[26] G.C. Borgia, R.J.S. Brown, P. Fantazzini, Uniform-penalty inversion of multiexponential decay data, J. Magn. Reson. 132 (1998) 65–77.
[27] L.W. Lake, Enhanced Oil Recovery, Prentice Hall, 1996.